Article type: Original Paper

Broadband 10 Gb/s operation of graphene electro-absorption modulator on silicon

Yingtao Hu[1], Marianna Pantouvaki[2], Joris Van Campenhout[2], Steven Brems[2], Inge Asselberghs[2], Cedric Huyghebaert[2], Philippe Absil[2] and Dries Van Thourhout[1]*

*Corresponding Author: E-mail: Yingtao.hu@intec.ugent.be

[1]Photonics Research Group, Department of Information Technology, Ghent University–IMEC, Sint-Pietersnieuwstraat 41, Gent， 9000, Belgium
[2]IMEC, Kapeldreef 75, Leuven, 3001, Belgium

Keywords: graphene, silicon modulator, integrated optical devices, optical interconnects, electro-absorption

Abstract: High performance integrated optical modulators are highly desired for future optical interconnects. The ultra-high bandwidth and broadband operation potentially offered by graphene based electro-absorption modulators has attracted a lot of attention in the photonics community recently. In this work, we theoretically evaluate the true potential of such modulators and illustrate this with experimental results for a silicon integrated graphene optical electro-absorption modulator capable of broadband 10 Gb/s modulation speed. The measured results agree very well with theoretical predictions. A low insertion loss of 3.8 dB at 1580 nm and a low drive voltage of 2.5 V combined with broadband and athermal operation were obtained for a 50 μm-length hybrid graphene-Si device. The peak modulation efficiency of the device is 1.5 dB/V. This robust device is challenging best-in-class Si (Ge) modulators for future chip-level optical interconnects.

1. Introduction

Integrated optical modulators with high modulation speed, small footprint, low power consumption and large operation bandwidth are highly desired to realize high-density low-power optical interconnects for future data centers and high performance computing systems [1, 2]. Mach-Zehnder interferometer (MZI) and ring resonator based silicon modulators exploiting the plasma dispersion effect were extensively optimized over the past few years [3-

6] and play a critical role in silicon transceiver prototypes emerging now [7-9]. However, MZI based modulators suffer from a large footprint, typically a few millimeters [6], and ring or disk modulators exhibit a narrow optical bandwidth, making them difficult to control and sensitive to temperature variations or fabrication errors [5]. Ge or SiGe electro-absorption modulators (EAM) are a promising alternative for these plasma dispersion based modulators. They can be compact and provide broadband operations but have limited thermal stability [10-12].

Graphene, a single layer of carbon atoms arranged in a honeycomb, is known to exhibit a variety of exceptional electronic and photonic properties [13, 14]. Due to its unique linear and gapless band dispersion, a single layer of graphene exhibits absorption of 2.3% for vertical incident light, for wavelengths ranging from the UV to the far infrared. By integrating a graphene monolayer onto an optical waveguide, light travelling in the waveguide can almost completely be absorbed. Moreover, shifting the Fermi level, with an external electric field or through chemical doping, allows tuning the absorption level, through Pauli blocking. This feature was first exploited in [15] to realize a compact waveguide integrated amplitude modulator and since then graphene modulators have attracted increasingly more attention in the photonics community, both in theoretical work and in experimental demonstrations [16-21]. Broadband operation, ultra-high speed modulation (>100 GHz), compact footprint and low power consumption (~fJ/bit) have been projected. However, current demonstrations are far from these predictions. While in [22] a ring resonator based graphene modulator exhibiting a bandwidth of 30GHz was demonstrated, this device scarifies one of the most important advantages of graphene – broadband operation. In this paper we theoretically investigate the true potential of silicon waveguide integrated graphene modulators and confirm these results experimentally, through the demonstration of a broadband 10 Gb/s operation in such a device. The realized graphene modulator is 50 μm long and based on a 750 nm-width silicon rib TM waveguide. The insertion loss is as low as 3.8 dB at 1580 nm.

The peak modulation efficiency reaches 1.5 dB/V and the device shows stable modulation depth from 20℃ to 49℃ (limited by the experimental setup). The electro-optical bandwidth was measured to be 5.9 GHz, allowing for open eye diagrams up to 10 Gb/s at drive voltages as low as 2.5 V and for wavelengths ranging from 1530 nm to 1565 nm, limited only by the bandwidth of the grating couplers and the optical amplifier used in the experiment. These results match well with the theoretical predictions providing confidence in the models and the proposed routes for further improvement.

2. Design and fabrication of graphene modulator

A typical single layer graphene modulator on silicon is configured as a graphene-oxide-silicon (GOS) structure, as shown in Figure 1. A rib structure allows contacting the silicon waveguide through the thin slab layer. The device is planarized with oxide to ease pasting the graphene layer (see next section). Three separately optimized doping levels are used to reduce the silicon contact resistance and the doped silicon contributed resistance of the device. To optimize the device performance we studied the influence of the rib waveguide dimensions, doping profile, gate oxide thickness and contact resistance on its modulation efficiency and bandwidth. The main target thereby is to maximize the interaction between the optical field and the graphene layer and to minimize the capacitance, allowing for high speed operation.

The absorption of graphene is usually derived from its 2D complex optical conductivity $\sigma_g(\omega, \mu c, \Gamma, T)$, calculated from the Kubo formula [23, 24]. It includes interband and intraband absorption and depends on the light angular frequency ω, chemical potential μ_c, charged particle scattering rate Γ, and temperature T. The complex permittivity can be calculated from the optical conductivity as $\varepsilon_g(\omega) = \varepsilon_0 + \frac{j\sigma_g}{\omega d_g}$, in which ε_0 is the dielectric constant of vacuum and d_g= 0.7 nm is the equivalent thickness of a single graphene layer. The scattering rate is strongly dependent on the graphene quality. Imperfections in the graphene layer induce density inhomogeneities, varying the optical conductivity across the

graphene sheet [25]. In the following calculations, we vary the scattering rate value to study the influence of the graphene quality on the modulator performance. Figure 2(a) shows the calculated dielectric permittivity as function of the chemical potential, assuming scattering rates $\hbar\Gamma$ = 0.43 meV and 15 meV ($\hbar$ is the reduced plank constant) at room temperature of T = 298 K and for a fixed wavelength of 1550nm. Note the graphene changing its character from "metallic" to "dielectric" at the "transition chemical potential" point μ_{ct} = 0.515 eV. Especially in the range of μ_c > 0.25 eV, different scattering rates lead to considerably different values for the dielectric constant. The resulting complex refractive index is shown in Figure 2(b). We calculated the modal absorption for the graphene covered silicon waveguide as function of its width using a commercial finite element solver (COMSOL multiphysics), taking into account the refractive index of graphene (2.137 + j1.888) at μ_c = 0 eV for $\hbar\Gamma$ = 15 meV. Given the anisotropic nature of the 2D-material, only in-plane components of the electric field are considered to interact with the graphene layer. It is important to note that this simulation model, using an equivalent thickness of graphene, leads to similar results as that using the surface current model [18], as we verified through direct comparison. The results for both the TE-like and TM-like mode of a rib waveguide with fixed height of 220 nm and slab thickness of 60 nm are plotted in Figure 3(a). The gate oxide thickness is varied from 1 nm to 20 nm. The absorption for the TM-like mode is clearly larger than that for the TE-like mode. While the absorption of the TE-like mode varies strongly with the gate oxide thickness but is rather independent of the waveguide width the opposite is true for the TM-like mode, reaching its maximum value for a width around 750 nm. This behavior results from the changing overlap between the graphene layer and the optical mode profile when changing the geometry of the waveguide.

In Figure 3(b) we plot the absorption for the TM mode as function of the chemical potential for the optimized waveguide with width of 750 nm and for scattering rates equal to 0.43, 15, 30 and 50 meV. It can be seen that the absorption of graphene can be tuned from ~0.15

dB/μm to almost transparent (<0.02 dB/μm) by increasing the chemical potential, with the transition almost completely taking place in the range $\mu_c = 0.25$ eV to $\mu_c = 0.55$ eV. For lower quality graphene, i.e. for higher scattering rates, full transparency cannot be reached and the insertion loss of the modulator will be larger.

To relate the absorption level to the gate voltage applied over the GOS structure we express the latter as function of the carrier density n_s in the graphene film:

$$V = -V_0 + \frac{d_{ox}e}{\varepsilon_{ox}} n_s \quad (1)$$

with V_0 the offset voltage originating from the natural doping in a real graphene sheet and ε_{ox} the dielectric constant of the oxide layer [26]. The carrier density n_s is a direct function of the graphene chemical potential [18], allowing us now to plot the TM mode absorption as function of the gate voltage as shown in Figure 3(c). We hereby assumed $V_0 = 0$ V and a scattering rate of $\hbar\Gamma = 15$ meV. The curves are symmetric around 0 V and the absorption decreases both for positive and negative applied voltages. To increase the modulation efficiency at zero bias voltage, a non-zero offset voltage V_0 can be induced by natural or artificial doping of the film. Also decreasing the gate oxide thickness helps to decrease the required drive voltage. However, it will also increase the capacitance of the GOS-stack, impacting the modulation bandwidth. As such there is an obvious trade-off between voltage modulation efficiency and high speed performance. To quantify this trade-off, we defined an equivalent circuit model for the modulator, shown in Figure 4. The GOS-structure is approximated as a lumped device with capacitance C_{GOS}. The total series resistance R_s comprises the silicon-metal contact resistance $R_{Si,c}$, the resistance of the doped silicon layers R_{Si}, the graphene sheet resistance R_g (measured from the side of the metal contact to the center of the waveguide) and the graphene-metal contact resistance $R_{g,c}$. The total capacitance C_{GOS} of the GOS structure consists of the oxide capacitance C_{ox}, the quantum capacitance of the graphene layer $C_{g,\,qua}$ [19] and the capacitance of the surface space charge layer in silicon C_s.

$$\frac{1}{C_{\mathrm{GOS}}} = \frac{1}{C_{ox}} + \frac{1}{C_{g,qua}} + \frac{1}{C_s} \quad (2)$$

Combining the definition of the quantum capacitance per unit area of the graphene [19] and the relationship between carrier density n_s and Fermi level[26], $C_{g,\ qua}$ can be calculated as:

$$C_{g,qua} = \frac{2e^2\sqrt{n_s}}{\hbar v_F\sqrt{\pi}} A \quad (3)$$

with A the area of the GOS structure. Realistic values for the graphene sheet resistance (R_g = 313 Ω/□) and contact resistance ($R_{g,c}$= 2400 Ω.µm) were estimated from TLM experiments. R_{Si} contains the resistances of the low density doped waveguide core, the moderately doped slab area and the highly doped silicon contact area taking into account their relative thickness. The actual values were calculated from experimental extracted sheet resistances of 1117 Ω/□ for the 220nm thick n doped (4×10^{18} cm^{-3}) waveguide core, 1920 Ω/□ for the 70nm thick n+ doped (3×10^{19} cm^{-3}) slab area and 48 Ω/□ for the 220nm thick n ++ doped (1×10^{20} cm^{-3}) silicon contact area.. The contact resistance on the n++ doped silicon was experimentally determined ($R_{Si,c}$ = 4.25 Ω). Further we assumed the waveguide to be 750 nm wide, the slab to be 2 µm wide and the distance between the n+ doping region and the edge of the lower doped waveguide to be 300 nm. The distance between the metal pads and the waveguide edge is assumed to be 2 µm, to avoid additional absorption losses. For simplicity, we assume that the graphene layer is undoped (n_s = 0) and hence $C_{g,\ qua}$ = 0. C_{ox} is calculated using a simple parallel capacitor model and to calculate the capacitance C_s associated with the space charge layer we assume a MOS capacitor model in depletion mode at 0 V gate voltage [27]. The parasitic elements in the circuit are based on empirical values [4, 28]. The actual values for the total series resistance and capacitance depend on the device length and the gate oxide thickness. For a device length of 50 um and oxide thickness of 5 nm, we find R_s = 155 Ω, C_{ox} = 259 fF and C_s = 128 fF. The total capacitance is then C_{GOS} = 85.8 fF. The associated 3-dB bandwidth is then calculated to be 8.3 GHz. Figure 5 plots this 3-dB bandwidth as function of the gate oxide thickness, for different values of the device length. This figure also shows the

modulation efficiency of the device. The latter is determined by dividing the modulation depth ($\alpha_{0.25\ eV}$ - $\alpha_{0.55\ eV}$)L with the voltage ΔV necessary for tuning the chemical potential from μ_c = 0.25 eV to 0.55 eV, equivalent to ~90% modulation of the absorption level in the graphene layer. For a given device length, the bandwidth linearly improves with increasing oxide thickness. The modulation efficiency however strongly degrades. Increasing the length improves the modulation efficiency but decreases the bandwidth. A gate oxide thickness of 5 nm and a device length of 50 μm seems a good compromise for realizing a modulator capable for operation at 10 GB/s. Further improving the device performance would require decreasing the series resistance, by reducing the sheet resistance, the contact resistance or the resistance of the doped silicon layers. The former two strongly rely on the quality of the transferred graphene and the contact technology where there is certainly still room for improvement [29, 30]. To verify our model, we fabricated graphene modulators on a 200-mm SOI wafer with 2 μm buried oxide and 220 nm top silicon layer. First, the Si rib waveguides were defined by two Si patterning and dry etching steps in a 130 nm CMOS processing line. After chemical-mechanical planarization (CMP), three phosphorous ion implantation steps were carried out to reduce device resistance. Next, a 5 nm thick silicon oxide was thermally grown on top of the Si waveguide and the wafer was diced. Subsequently, a single-layer graphene sheet grown by chemical vapor deposition (CVD) on a Si/SiO_2/Cu substrate was transferred to the diced Si chips using an elastomer stamp [31]. The graphene was patterned by photolithography followed by an oxygen plasma etch. Two separate steps created the graphene-metal contact (10 nm Cr/50 nm Au/20 nm Ti/420 nm Au) and the Si-metal contact (20 nm Ti/480 nm Au). Optical microscope and SEM images of the fabricated devices are shown in Figure 6.

3. Device DC performance

Fiber-to-fiber transmission measurements for unbiased graphene EAM devices with lengths of 50 μm, 100 μm, 150 μm and reference waveguides without graphene coverage were carried

out for devices optimized both for TM (W = 750 nm) and TE (W = 500 nm) polarization. A modal absorption of ~0.11 dB/μm and ~0.06 dB/μm were extracted for the TM and TE rib waveguides respectively, over a wavelength range of 80 nm around 1560 nm (limited by the tunable laser and the grating couplers used for coupling light into the chip), as shown in Figure 7(a). The extracted absorption values are slightly lower than the calculated values at μ_c=0 eV (~0.155 dB/μm for TM and ~0.7 dB/μm for TE) but equals to the value around μ_c = 0.37 eV according to Figure 3(b), which could be explained by assuming that the graphene after full device processing is lightly p-doped, shifting the neutrality point. Figure 7(b) shows the transmission through a 50 μm long device optimized for TM-polarization, for a drive voltage increasing from -4 V to 4 V. The spectral response is mainly determined by the wavelength dependence of the grating coupler used for coupling light into the waveguide, as can be seen from the reference waveguide transmission. The inset shows the resulting extinction ratio (ER) calculated from these curves. In Figure 7(c), we plotted the normalized transmission versus applied voltage (modulation curve) for devices with lengths of 50, 100 and 150 μm at the TM grating coupler's peak coupling wavelength of 1580 nm. It can be seen that 5.2 dB extinction ratio (ER) from -4 V to 4 V and only 3.8 dB of on-state insertion loss (IL) is obtained for the 50 μm-length device. Larger ERs of 7.4 dB and 10.6 dB are obtained for the 100 μm and 150 μm long devices respectively, but these exhibit larger insertion losses also. As our calculations in the previous section show (Figure 3), this could be explained by imperfections in the graphene film. From comparing the transmission of the modulator at a bias voltage of 4V (-16.4, -20.9 and -24.8 dB for 50, 100 and 150 μm long devices respectively) with that of a reference waveguide (-12.7dB), we obtain a residual absorption of 0.08 dB/μm for the modulator at its transparency point. Similarly, at a bias voltage of -4 V corresponding to the neutrality point μ_c = 0 eV the respective transmission values are -21.6, -28.3 and -35.4 dB, equivalent with an absorption of 0.15 dB/μm. This absorption value agrees very well with the predicted value in Figure 3(b). The fact that the neutrality point has

shifted to a negative bias voltage again indicates the graphene layer is p-doped. Figure 5(d) shows the ILs and modulation efficiencies at different applied voltages. The highest modulation efficiency, 1.5 dB/V, is observed at -1 V.

To study the temperature dependence of the operating characteristics, we tested the 50 μm-length device at chip temperatures of 20 ℃, 30 ℃ and 49 ℃. Figure 8(a) shows the modulation curves at 1560 nm for the three different chip temperatures, showing no significant temperature dependence. Figure 8(b) shows the $ER_{-4V\sim4V}$ for the full wavelength range spanning from 1520 nm to 1600 nm, again indicating good temperature tolerance across the full tested wavelength range. To fully understand this behavior we simulated the on-off curves for temperatures ranging up to 175°C, taking into account the temperature dependence of the optical conductivity. The results are shown in Figure 8(c), illustrating again the weak temperature dependence with only a slight decrease of the steepness of the curves. To quantify this we calculated the ER = $(\alpha_{0.25\ eV} - \alpha_{0.55\ eV})L$ of a 50 μm length device as a function of temperature. As shown in Figure 8(d) the ER is expected to decrease with increasing temperature but only by 0.0013 dB/℃ around 25 ℃ and by 0.0028 dB/℃ around 175 ℃. When the temperature raises 100 ℃ above room temperature the decrease in ER is ~0.018 dB which is negligible.

4. Small-signal RF characterizations

The electrical S-parameters of the 50 μm long modulator were measured from DC up to 20 GHz with a vector network analyzer. The measured *S11* phase and magnitude at 0 V bias are plotted in Figure 9. From fitting these to the equivalent circuit model of Figure 4, a series resistance R_s of 241 Ω and device capacitance C_{GOS} of 81.8 fF can be extracted. The associated electrical 3-dB bandwidth is estimated to be 6.1 GHz (at 0 V) [32]. Similarly, the electrical 3-dB bandwidth measured at -1 V and -2V bias is 5.8 GHz and 2.7 GHz respectively. The degradation in bandwidth with forward bias is related to the associated increase in capacitance, as extracted from the curve fitting (see table 1) and CV-

measurements [32]. The extracted values are also in good agreement with our model: at 0V, corresponding with a chemical potential of 0.37 eV as estimated from DC characterization of the device and the silicon in depletion mode, $C_{g,\ qua}$ and C_s are calculated to be 366 fF and 128 fF respectively. Together with C_{ox} = 259 fF, the total modulator capacitance is estimated to be 69 fF. At 2V, the chemical potential is shifted to 0.49 eV so that $C_{g,\ qua}$ increases to 482 fF. The silicon now operates in accumulation mode so that C_s increases to infinity. In this case the total capacitance is 169 fF. These calculated values are very close to the values extracted from the measurement. The electro-optical (E-O) response was measured with the same system. The results, for different bias voltages, are shown Figure 10 as $S21^2$. The E-O response 3-dB bandwidth is 5.9 GHz at 0 V, 5.3 GHz at -1 V and 2.6 GHz at 2 V. The measured E-O bandwidth matches well with the electrical 3-dB bandwidth estimated from the equivalent circuit by fitting the measured *S11* proving the proposed equivalent circuit accurately represents the device's electrical high speed performance. Overall it is clear the device response is limited by its electrical bandwidth and not by the intrinsic speed of the material.

5. Eye-diagram measurements

To demonstrate the ability to efficiently transmit digital data, eye diagram measurements were carried out for the 50 μm-length device. Wide open eye diagrams with dynamic ER ~ 2.5 dB and low jitter were obtained at 6 Gb/s and up to 10 Gb/s with a drive voltage of 2.5 V_{pp} and 1.75 V forward bias at working wavelength of 1560 nm, as shown in Figure 9. Further, we measured the eye diagrams at 10 Gb/s for different wavelengths ranging from 1530 nm to 1565 nm. Wide open and clear eye diagrams with a dynamic extinction ratio of 2.3 dB or better were obtained for all wavelengths. The operation bandwidth actually is limited by the envelope of the grating couplers used to couple the light into the device, the available tunable laser and optical filters used in the measurements and not by the modulator itself, which has the potential to operate over a much larger optical bandwidth [15]. The dynamic energy consumption is estimated to be ~350 fJ/bit ($E_{bit} \sim CV^2/4$) and the static power consumption is

calculated to be <10^{-4} mW, taking into account the ~10^{-1} nA leakage current measured [32]. Finally, we compare the most relevant performance metrics to state-of-the-art Si and Ge modulators in Table 2, illustrating the benefits of the graphene EAM in terms of thermal properties, optical bandwidth and footprint. The transmitter penalty (TP), which combines the effects of extinction ration and insertion loss, allows to compare these different devices. At this moment the TP of Ge electroabsorption modulators and silicon ring resonators is still better than the TP for our graphene modulator. However, the latter is the only device that allows operation over a large optical bandwidth. As the operation speed of the graphene modulator currently is limited by the RC delay, further design optimizations should focus on reducing device series resistance R_s and capacitance C_{GOS}. There are a lot of strategies to reduce R_s: shrinking the distance between metal pad and waveguide (current value is 2 μm), increasing doping density in the slab area, increasing the thickness of the slab, improving the graphene quality and thus reduce the resistance contribution of the graphene sheet between metal pad and the GOS capacitor and using improved metal-graphene contact technologies [30]. Implementing these improvements, R_s potentially can be reduced from the current value of 241 Ω to less than 50 Ω. Combining this improved resistance value with the current device capacitance (~80 fF), an electrical bandwidth of 18 GHz can be expected. Using a double graphene layer approach as proposed in [17], the extinction ratio (in dB/um) can be roughly doubled allowing to shorten the device, decrease the capacitance and hence further increase the electrical bandwidth. It is promising that modulation speed of 25 Gb/s and beyond could be realized.

6. Conclusion

In conclusion, we propose a theoretical model for a graphene-on-silicon electro-absorption modulator and verify this model experimentally. Fabricated devices perform well, in good agreement with simulations. We demonstrated a compact graphene-Si electro-absorption modulator operating up to 10 Gb/s over a broad wavelength range. The operating

characteristics remain virtually unaltered for temperatures up to 49°C. The static power consumption of a 50 μm long device is less than 1×10^{-4} mW and the dynamic power consumption is ~350 fJ/bit. As such the device is challenging best-in-class Si (Ge) modulators for future chip-level optical interconnects. From the model, further improvement is expected through improving the graphene film quality and decreasing the device series resistance.

Acknowledgements (This work was supported by imec's Core Partner Program. This work was partially supported by the ERC-project ULPPIC. Prof B.J. Cho (KAIST, Korea) is greatly acknowledged for the generous supply of high-quality graphene. Thank Weiqiang Xie for the contribution of SEM characterization).

Received: ((will be filled in by the editorial staff))
Revised: ((will be filled in by the editorial staff))
Published online: ((will be filled in by the editorial staff))

References

1. Reed, G., et al., *Silicon optical modulators.* Nature Photonics, 2010. **4**(8): p. 518-526.
2. Young, I.A., et al., *Optical I/O technology for tera-scale computing.* Solid-State Circuits, IEEE Journal of, 2010. **45**(1): p. 235-248.
3. Xiao, X., et al., *25 Gbit/s silicon microring modulator based on misalignment-tolerant interleaved PN junctions.* Optics express, 2012. **20**(3): p. 2507-2515.
4. Hu, Y., et al., *High-speed silicon modulator based on cascaded microring resonators.* Optics express, 2012. **20**(14): p. 15079-15085.
5. Timurdogan, E., et al., *An ultralow power athermal silicon modulator.* Nature communications, 2014. **5**.
6. Streshinsky, M., et al., *Low power 50 Gb/s silicon traveling wave Mach-Zehnder modulator near 1300 nm.* Optics express, 2013. **21**(25): p. 30350-30357.
7. Pantouvaki, M., et al. *8x14Gb/s Si Ring WDM Modulator Array with Integrated Tungsten Heaters and Ge Monitor Photodetectors*. in *Optical Fiber Communication Conference*. 2014: Optical Society of America.
8. Liu, Y., et al. *Ultra-compact 320 Gb/s and 160 Gb/s WDM transmitters based on silicon microrings*. in *Optical Fiber Communication Conference*. 2014: Optical Society of America.
9. Sun, C., et al. *A monolithically-integrated chip-to-chip optical link in bulk CMOS*. in *VLSI Circuits Digest of Technical Papers, 2014 Symposium on*. 2014: IEEE.
10. Feng, D., et al., *High speed GeSi electro-absorption modulator at 1550 nm wavelength on SOI waveguide.* Optics express, 2012. **20**(20): p. 22224-22232.
11. Gupta, S., et al. *50GHz Ge Waveguide Electro-Absorption Modulator Integrated in a 220nm SOI Photonics Platform*. in *Optical Fiber Communication Conference*. 2015: Optical Society of America.
12. Srinivasan, S.A., et al., *56Gb/s Germanium Waveguide Electro-Absorption Modulator.* 2015.
13. Bonaccorso, F., et al., *Graphene photonics and optoelectronics.* Nature Photonics, 2010. **4**(9): p. 611-622.

14. Avouris, P., *Graphene: electronic and photonic properties and devices.* Nano letters, 2010. **10**(11): p. 4285-4294.
15. Liu, M., et al., *A graphene-based broadband optical modulator.* Nature, 2011. **474**(7349): p. 64-67.
16. Mohsin, M., et al., *Graphene based low insertion loss electro-absorption modulator on SOI waveguide.* Optics express, 2014. **22**(12): p. 15292-15297.
17. Liu, M., X. Yin, and X. Zhang, *Double-layer graphene optical modulator.* Nano letters, 2012. **12**(3): p. 1482-1485.
18. Koester, S.J., H. Li, and M. Li, *Switching energy limits of waveguide-coupled graphene-on-graphene optical modulators.* Optics express, 2012. **20**(18): p. 20330-20341.
19. Koester, S.J. and M. Li, *High-speed waveguide-coupled graphene-on-graphene optical modulators.* Applied Physics Letters, 2012. **100**(17): p. 171107-171107-4.
20. Lu, Z. and W. Zhao, *Nanoscale electro-optic modulators based on graphene-slot waveguides.* JOSA B, 2012. **29**(6): p. 1490-1496.
21. Youngblood, N., et al., *Multifunctional graphene optical modulator and photodetector integrated on silicon waveguides.* 2014.
22. Phare, C.T., et al., *Graphene electro-optic modulator with 30 GHz bandwidth.* Nature Photonics, 2015. **9**(8): p. 511-514.
23. Hanson, G.W., *Dyadic Green's functions and guided surface waves for a surface conductivity model of graphene.* Journal of Applied Physics, 2008. **103**(6): p. 064302.
24. Gusynin, V., S. Sharapov, and J. Carbotte, *Sum rules for the optical and Hall conductivity in graphene.* Physical Review B, 2007. **75**(16): p. 165407.
25. Tan, Y.-W., et al., *Measurement of scattering rate and minimum conductivity in graphene.* Physical review letters, 2007. **99**(24): p. 246803.
26. Gosciniak, J. and D.T. Tan, *Theoretical investigation of graphene-based photonic modulators.* Scientific reports, 2013. **3**.
27. Hu, C., *Modern Semiconductor Devices for Integrated Circuits.* 2010.
28. Yu, H., et al., *Compact, Thermally Tunable Silicon Racetrack Modulators Based on an Asymmetric Waveguide.* 2013.
29. Smith, J.T., et al., *Reducing contact resistance in graphene devices through contact area patterning.* ACS nano, 2013. **7**(4): p. 3661-3667.
30. Leong, W.S., H. Gong, and J.T. Thong, *Low-Contact-Resistance Graphene Devices with Nickel-Etched-Graphene Contacts.* ACS nano, 2013. **8**(1): p. 994-1001.
31. Song, J., et al., *A general method for transferring graphene onto soft surfaces.* Nature nanotechnology, 2013. **8**(5): p. 356-362.
32. Y. T. Hu, M.P., S. Brems, I. Asselberghs, C. Huyghebaert, M. Geisler, C. Alessandri, R. Baets, P. Absil, and a.J.V.C. D. Van Thourhout, *Broadband 10gb/s graphene electro-absorption modulator on silicon for chip-level optical interconnects.* Electron Devices Meeting (IEDM), 2014 IEEE International., 2014.

Figure 1. (a) A 3 dimensional schematic drawing of a single layer graphene electro-absorption modulator (EAM) integrated on SOI platform. (b) Cross section of the graphene EAM.

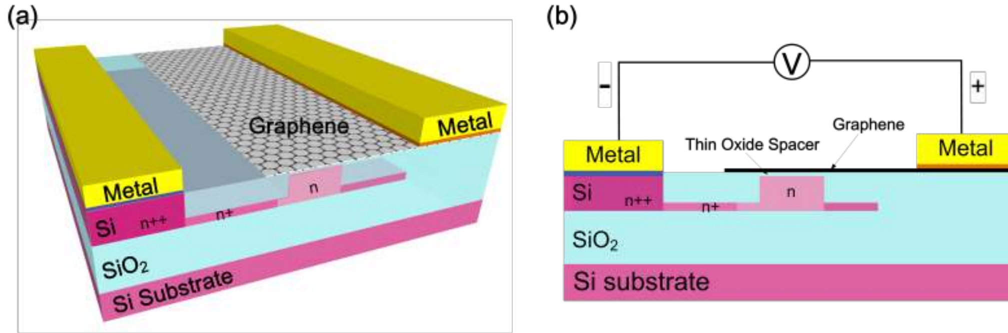

Figure 2. (a) Calculated complex dielectric constant (real part, imaginary part and magnitude) of graphene as a function of chemical potential at fixed wavelength of 1550 nm for $\hbar\Gamma = 0.43$ meV and 15 meV. (b) Calculated complex refractive index (real part, imaginary part) of graphene as a function of chemical potential at fixed wavelength of 1550 nm for $\hbar\Gamma = 0.43$ meV and 15 meV.

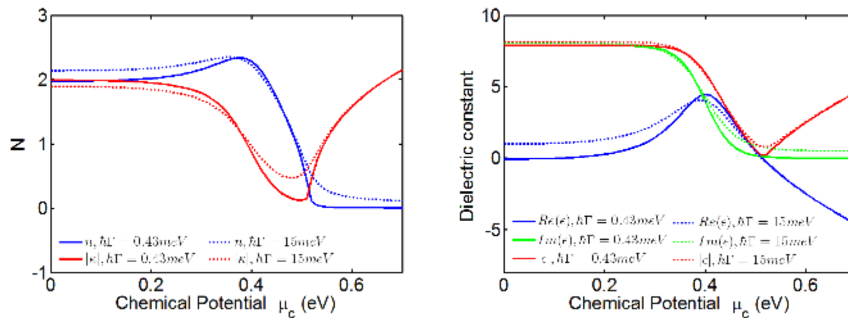

Figure 3. (a) Modal absorption of graphene-on-silicon waveguide for TE and TM mode as function of waveguide width for different oxide thickness. The height of the top silicon layer is 220 nm and the slab thickness is 60 nm. (b) TM mode absorption for the optimized waveguide with width of 750 nm at different chemical potentials from 0 to 0.7 eV and different scattering rates of $\hbar\Gamma = 0.43$, 15, 30 and 50 meV. (c) TM mode absorption at different voltages for different oxide thickness of 1, 5, 10 and 15 nm with scattering rate $\hbar\Gamma$ =15 meV and $V_0 = 0$ V. (d) TM mode absorption at different voltages for scattering rate $\hbar\Gamma$ =0.43, 15, 30 and 50 meV with $d_{ox} = 5$ nm and $V_0 = 0$ V.

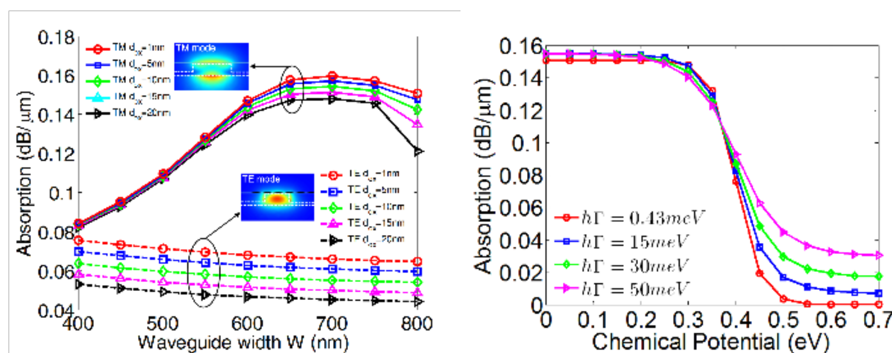

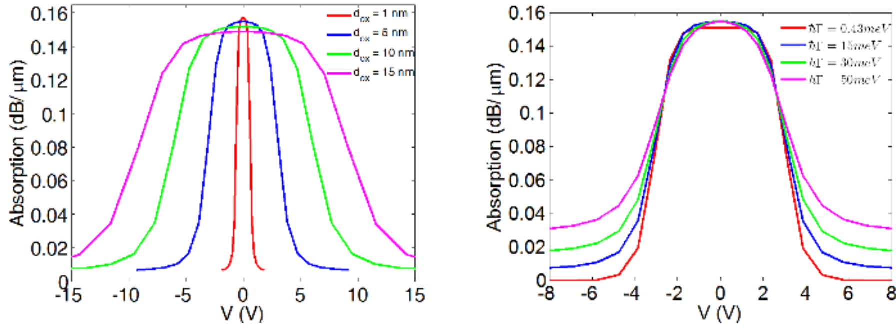

Figure 4. The equivalent electrical circuit for the proposed single layer graphene modulator. $R_{Si,c}$ is the silicon-metal contact resistance, R_{Si} is the resistance of the doped silicon, R_g is the resistance of the graphene sheet between metal and the waveguide edge, $R_{g,\,c}$ is the graphene-metal contact resistance, R_{sub} is the resistance of the substrate, C_{GOS} is the total capacitance of the GOS structure including the oxide capacitance C_{ox}, the quantum capacitance of the graphene layer $C_{g,\,qua}$ and the capacitance of the depletion-layer of silicon C_S, C_{air} is the capacitance between two metal pads through the air, C_{box} is the capacitance of the buried oxide layer.

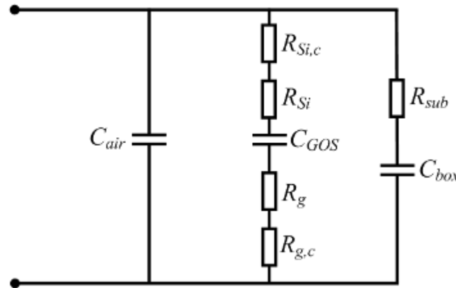

Figure 5. Calculated modulation efficiencies and electrical 3-dB bandwidths as functions of the thickness of the oxide spacer for different device length of 50, 100 and 150 μm.

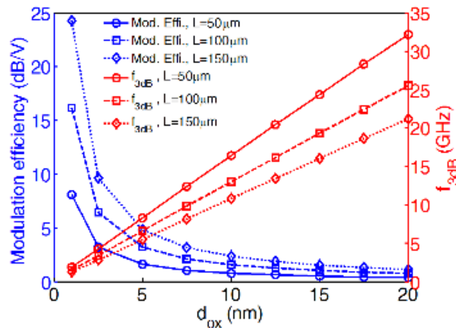

Figure 6. (a) Optical microscope image of the fabricated graphene EAMs with TM grating couplers for fiber-to-chip optical coupling. (b) Top-view and (c) tilted-view SEM images of fabricated devices.

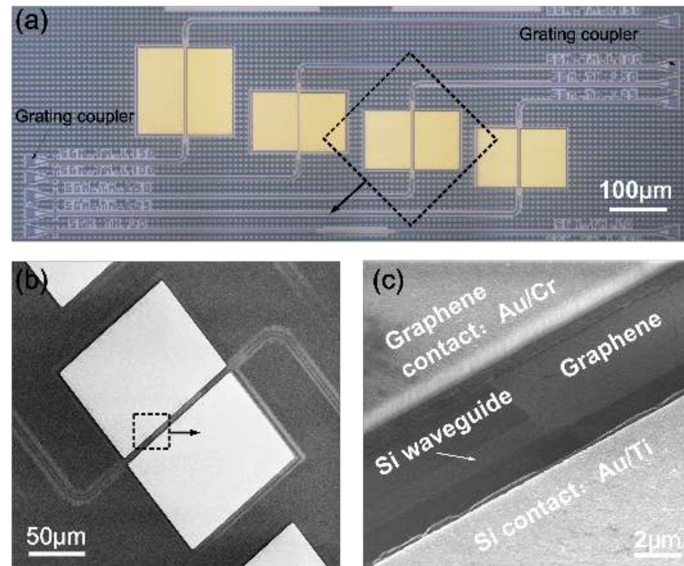

Figure 7. (a) Extracted graphene absorption loss of ~0.11 dB/μm and ~0.06 dB/μm for TM 750 nm-width and TE 500 nm-width waveguides across the full measured wavelength range from 1520 nm to 1600 nm (at bias 0 V). (b) Fiber-to-fiber transmission spectra of the 50μm TM graphene EAM at different drive voltages. (c) Normalized transmission versus applied voltage (modulation curve) for device lengths of 50, 100 and 150 μm at the TM grating coupler's peak coupling wavelength of 1580 nm. (d) The IL and modulation efficiency for the 50 μm device at different applied voltages.

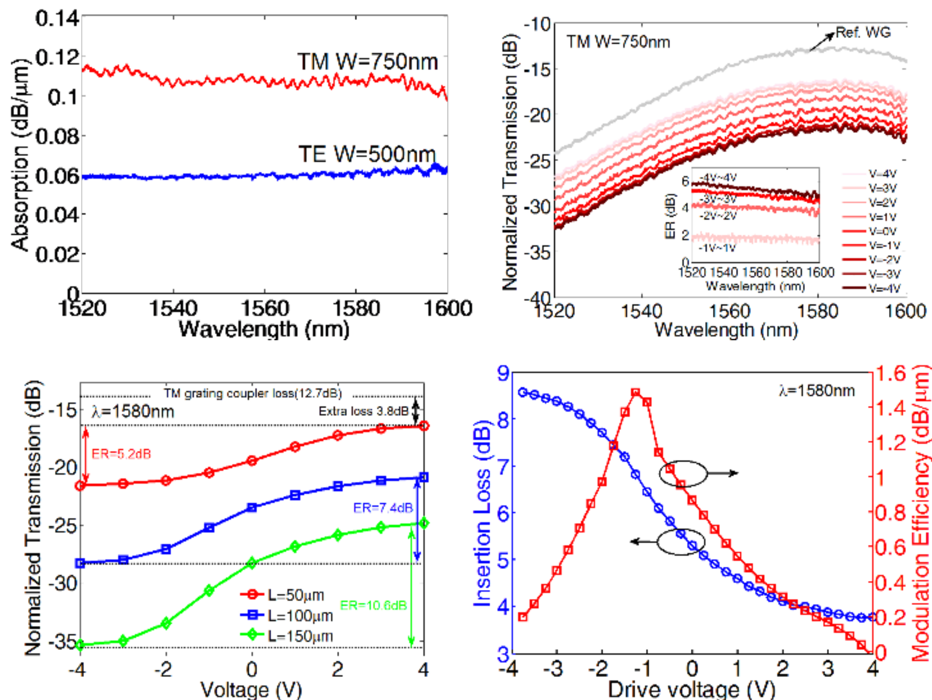

Figure 8. (a) The measured modulation curves versus applied voltage at 1560 nm. (b) Static extinction ratio versus wavelength of a 50 μm TM graphene EAM measured for -4 V to 4 V voltage swing at chip temperatures of 20 ℃, 30 ℃ and 49 ℃. (c) Calculated TM mode absorption of graphene at different temperature of 25 ℃, 75 ℃, 125℃ and 175℃. (d) Calculated ER of a 50 μm length device as a function of temperature.

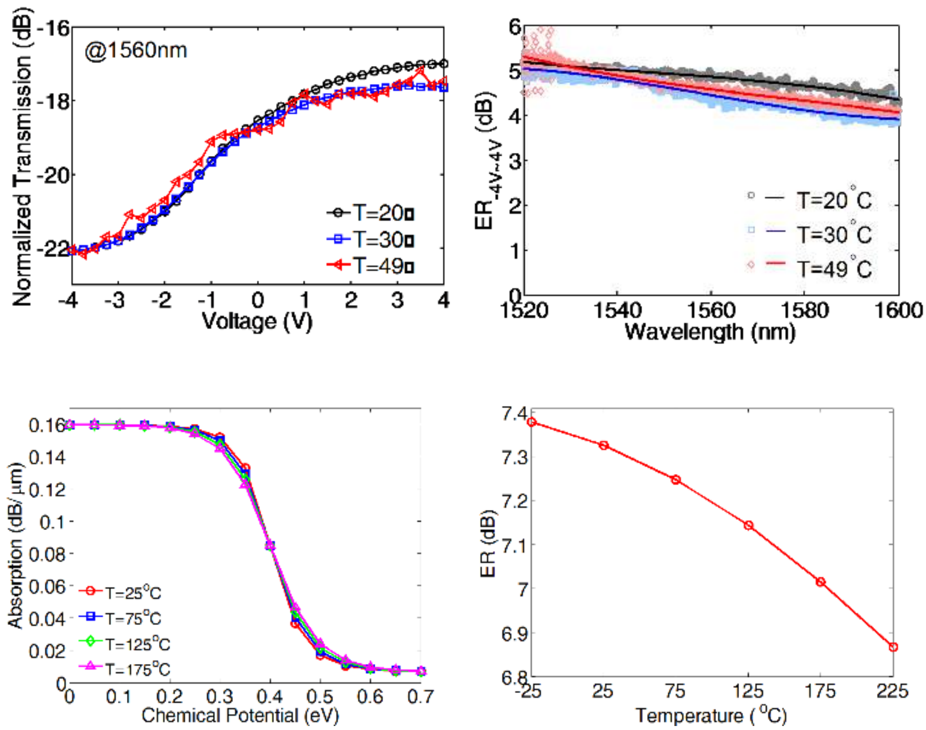

Figure 9. Measured RF *S11* response of the 50 µm graphene EAM at 0 V bias and the fitted curves using an equivalent electrical circuit model.

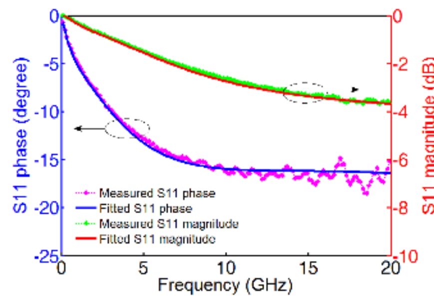

Figure 10. Measured and normalized electro-optical *S21* responses of the 50 µm graphene EAM at different bias voltages showing electro-optical bandwidth of 5.9 GHz in reverse bias and 2.6 GHz in forward bias.

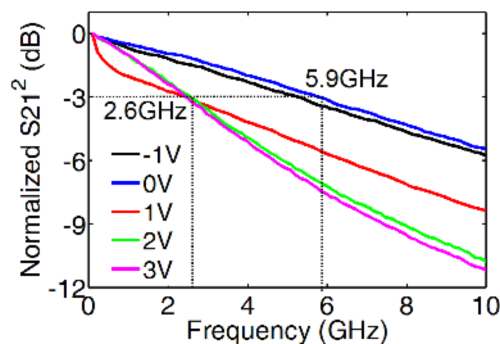

Figure 11. Optical eye diagrams measured at 1560 nm for the 50 µm graphene EAM device at 6 Gb/s, 8 Gb/s and 10 Gb/s modulation speed, using a drive voltage of 2.5 V_{pp} swing and 1.75 V forward bias delivered with a 50 Ω terminated probe.

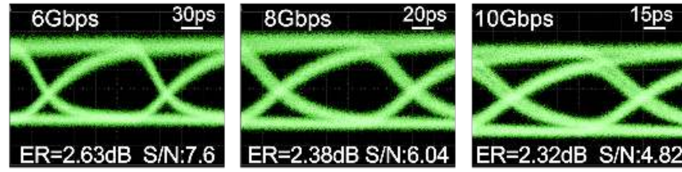

Figure 12. Optical eye diagrams measured at 10Gb/s modulation speed for the 50µm graphene EAM device for wavelengths in the range 1530-1565 nm, using a drive voltage of 2.5 V_{pp} swing and 1.75 V forward bias delivered with a 50 Ω terminated probe. A dynamic extinction ratio of 2.3 dB or better is obtained for all wavelengths.

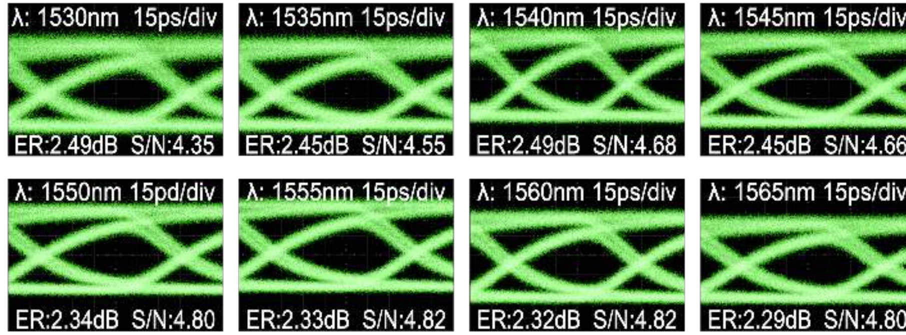

Table 1. The Series resistance R_s, device capacitance $C_{GOS,}$ the electrical 3-dB bandwidth $f_{3dB,e}$ and E-O response bandwidth $f_{3dB,e\text{-}o}$.

Bias [V]	R_s [Ω]	C_{GOS} [fF]	$f_{3dB,e}$ [GHz]	$f_{3dB,e\text{-}o}$ [GHz]
-1V	269	78	5.8	5.3
0V	241	81.8	6.1	5.9
2V	246	194	2.7	2.6

Table 2. Benchmarking table comparing the performance of the graphene-Si EAM versus different types of state-of-the-art Si and SiGe optical modulators. The graphene EAM combines compact footprint with large optical bandwidth over a wide temperature range, with relatively low power consumption. Our work has substantially advanced the modulation speed of the graphene EAM over prior reports. Significant potential still exists to further improve the modulation speed of the graphene EAM closer to speeds obtained in highly optimized Si(Ge) modulators.

Modulator type	Ref.	Footprint [μm²]	Wavelength [nm]	Drive voltage [V]	Optical bandwidth [nm]	Temperature range [℃]	ER [dB	Insertion Loss [dB]	Transmitter Penalty‡ [dB]	Static Power [mW]	Dynamic Power [fJ/bit]	3dB frequency [GHz]	Maximum Bit Rate [Gb/s]
Si Mach-Zehnder Modulator	[6]	~3000x500	1300	1.5	>80*	>80*	3.4	7.1	15.5	~20#	450	30	50
Si Ring Modulator	[5]	~10x10	1550	0.5	<0.1	<1	6.4	1.2	7.5	<0.01	~1	21	44
SiGe EAM	[10]	~55x10	1550	2.8	35 5§	<1 <40§	~5	~4	11.1	>2.2	60	>30	28
SiGe EAM	[12]	~40 **x10**	1615	2.0	>22.5	n/a	3.3	4.9	13.4	1.2	12.8	>50	56
Graphene-Si EAM	[15]	~40x10	1500	3	>180	n/a	2.4	n/a	n/a	n/a	n/a	1.2	n/a
Graphene-Si EAM	[22]	80 x80	1550	7.5	<0.1	n/a	n/a	12.5	n/a	n/a	800	30	22
Graphene-Si EAM	This work	**~50x10**	1550	2.5	**>80**	**>29**	2.5	**3.8**	**13.4**	**<1x10^{-4}**	**350**	2.6-5.9	**10**

*Assuming balanced Mach-Zehnder modulator with broadband 3dB splitters, #Mach-Zehnder bias control, §Bandwidth can be traded for temperature tolerance, ‡The transmitter penalty is

defined as $TP=(P_{out}(1)-P_{out}(0))/(2\times P_{in})$ where $P_{out}(1)$ and $P_{out}(0)$ are the high and low level of output optical power from the modulator and P_{in} is the input optical power[12].

Graphical Abstract

Graphene is considered to be a promising material for realizing ultra-high bandwidth and broadband operation electro-absorption modulators. However, demonstration of a graphene based modulator combining both properties in a single device is still lacking. In this work, the true potential of silicon integrated single layer graphene modulators is theoretically investigated and a broadband modulator operating at 10 Gb/s is demonstrated. The realized graphene modulator is 50 µm long and based on a 750 nm-wide silicon rib TM waveguide. It exhibits an insertion loss of 3.8 dB at 1580 nm and a drive voltage of 2.5 V combined with broadband and athermal operation. The static power consumption is less than 1×10^{-4} mW and the dynamic power consumption is ~350 fJ/bit. These results match well with the theoretical predictions.